**Coupled Systems Mechanics**, *Vol. 4, No. 2 (2015) 137-155*
DOI: http://dx.doi.org/10.12989/csm.2015.4.2.137


# Homogenized elastic properties of graphene for moderate deformations

Eduard Marenić and Adnan Ibrahimbegovic*

*Sorbonne Universités / Université de Technologie de Compiegne*
*Chaire de Mécanique, Lab. Roberval de Mécanique,*
*Centre de Recherches de Royallieu 60203 Compiegne, France*

*(Received May 5, 2015, Revised June 2, 2015, Accepted June 7, 2015)*

**Abstract.** This paper presents a simple procedure to obtain a substitute, homogenized mechanical response of single layer graphene sheet. The procedure is based on the judicious combination of molecular mechanics simulation results and homogenization method. Moreover, a series of virtual experiments are performed on the representative graphene lattice. Following these results, the constitutive model development is based on the well-established continuum mechanics framework, that is, the non-linear membrane theory which includes the hyperelastic model in terms of principal stretches. A proof-of-concept and performance is shown on a simple model problem where the hyperelastic strain energy density function is chosen in polynomial form.

**Keywords:** graphene; elastic properties, molecular mechanics; homogenization

## 1. Introduction

Nanoscale systems and processes based on graphene Novoselov *et al*. (2005), Singh *et al*. (2011) are becoming more viable for engineering applications, however, our ability to model their performance remains limited. The main challenge is that parts of graphene-based devices modelled with discreet models (such as molecular mechanics (MM) and molecular dynamics (MD)) typically contain extremely large number of particles, even though the actual physical dimension may be quite small. For instance, a simple square shaped Single Layer Graphene Sheet (SLGS) with the side length of approximately 500 nm has already nearly one million of carbon atoms. Following explicitly the trajectory for large number of degrees of freedom easily becomes intractable. Thus we reach for a substitute, continuum model which models the average mechanical behaviour of atomic system.

Averaged continuum properties of graphene in the context of infinitesimal deformation is the subject of research for nearly 10 past years (e.g., see Caillerie *et al*. 2006, Reddy *et al*. 2006, Huang *et al*. 2006, Zhao *et al*. 2009, Georgantzinos *et al*. 2010). However, there is a large discrepancy in the results obtained by means of the different simulation methods and experimental

∗Corresponding author, Professor, E-mail: adnan.ibrahimbegovic@utc.fr
[a] Ph.D., E-mail: eduard.marenic@utc.fr


http://www.techno-press.org/?journal=csm&subpage=7 ISSN: 2234-2184 (Print), 2234-2192 (Online)

studies (e.g. see Reddy *et al.* 2006, Huang *et al*. 2006). We reported also in Marenić *et al*. (2013) an overview of the mechanisms causing the result scattering which can be summarized as: formulation differences (which concerns MM, MD, *ab initio* methods, continuum mechanics); choice of interatomic potential driving the atomic system (Tersoff-Brenner Tersoff 1986, Brenner 1990) usually, also Morse Morse (1929), AMBER and second generation REBO Brenner *et al*. 2002); uncertainty of the thickness (yet known as Yakobson's paradox) Huang *et al.* (2006); and also size effect, relaxation (minimisation of the energy due to coordination), chirality, and edge passivation Lu *et al.* (2011). In Marenić *et al*. (2013), we also pointed out the influence of the boundary conditions on the (linear-elastic) stiffness of SLGS, which is related to the homogenized stiffness bounds as introduced in Huet (1990) and latter discussed in Markovic and Ibrahimbegovic (2004).

We tend here to give a combined MM and continuum approach for the study of the in plane mechanical behaviour of SLGS under large deformations. In other words we present equivalent continuum modelling of large deformations of graphene, which goes beyond what linear theory can handle. We note here that continuum models of nano-structures are extremely simplified, however they bring insight as well as quantitative information on the relevant physical phenomena. Thus, these models seam optimal for the current and potential future applications of graphene materials, such as, e.g., reinforcement agents to strengthen composites or structural parts. Recently, graphene has attracted both academic and industrial interest in graphene-based polymer nanocomposites because it can produce a dramatic improvement in properties at very low filler content. Thus it can be used either in graphene-based nano-electro-mechanical systems (NEMS) devices Geim and Novoselov (2007), or graphene-conducting polymer nanocomposites (see Hu *et al*. 2014, Stankovich *et al*. 2006, Gmez *et al*. 2011). Micro-mechanical models are conveniently used to predict macroscopic properties of conventional reinforced polymer composites, which behave as heterogeneous material (Mori and Tanaka 1973) on the scale somewhat higher than the nano length scale. However, when the multi-scale model has a goal to predict properties of nano-reinforced composites, a detailed knowledge of the response on the scale of the nano-structure is required (see an example of the multiscale approach for the nano-clay reinforced polymer Bedoui and Cauvin 2012, Gelineau *et al.* 2015). Similarly for the graphene-based nanocomposites, and mentioned application, the mechanical response of graphene under different loading programs, boundary conditions and large strain regime is crucial, and should still be better understood. Experimental investigation (see e.g. Lee *et al*. 2008) and first-principles calculations show that graphene undergo very large deformations, with highly nonlinear behavior and still remain elastic, with stable bonds and intact bond topology. This fact allows us to adapt and use a finite strain elastic model for the large range of phenomena and motivates us to benefit from somewhat simplified nonlinear membrane theory. The main difficulty in constructing the solutions for the problems of the deformable body subjected to large deformations concerns the choice of the suitable formulation like Lagrangian, Eulerian, updated Lagrangian, etc. Choosing a particular formulation implies the corresponding choice of the reference frame and the properly invariant measure of large strain Ibrahimbegovic (2009), Wriggers (2008), Belytschko *et al*. (2000). There are generally two ways of dealing with this problem. First considers the theoretical development placed in the framework of differential manifolds Abraham and Marsden (1987) which enables the switch between configurations by means of the metric tensor. However, the conceptual clarity of the theoretical formulation of the finite deformation elasticity set on a differential manifold does not imply simplicity with respect to numerical implementation, mainly due to locking. In Arroyo and Belytschko (2002) a general methodology to develop hyper-elastic membrane models for

single-atomic-layered films is presented with an extension of the Cauchy-Born (CB) rule Ericksen (1984) Zanzotto (1996), Ericksen (2008) based on the exponential map. The exponential map is added in the formulation as an extension of CB rule to account for the curvature of the lattice vectors. Thus, they are using curvilinear coordinates and give general formulation capable to treat even buckling problems of carbon nano tubes. In this paper we are performing virtual experiments (MM simulation) on the representative sample of the graphene lattice and thus we are not making any assumption regarding the kinematics of the atoms (CB hypothesis does not have to be fulfilled). These virtual experiments are used to fit energy potential. Similar procedure is performed in e.g., Reddy *et al*. 2006, Lu and Huang (2009), Cadelano *et al*. 2009, Lu *et al*. 2011, where only uniaxial tests are performed giving an elastic potential with respect to nominal strain. In Cadelano *et al.* 2009 continuum elasticity theory and tight-binding atomistic simulations are combined to determine the constitutive nonlinear stress-strain relation, and the corresponding nonlinear elastic moduli for graphene. We show here biaxial tests and, moreover, we seek to adopt the nonlinear membrane theory which includes, as a special case, the hyperelastic model in terms of principal stretches. The latter was often used to characterise rubber-like materials, see Ibrahimbegovic and Gruttmann (1993) with finite element formulation of elastic membrane shells with co-axial energy-conjugate pairs of stress and strain measures. The main advantage of the formulation in Ibrahimbegovic and Gruttmann (1993) pertains to the finite element analysis of elastic membranes. The problem of the finite deformation of elastic membranes can be solved relaying on the Cartesian structure without going to a more general setting of manifolds (note that this is not possible for the elastoplastic membranes Ibrahimbegovic 1994). As a first step, we present the modelling of the in plane large deformation of SLGS, however the proposed theory can be extended to membranes whose reference and current configurations can be arbitrary space-curved surfaces. Thus, the development of homogenized constitutive model is based on the well-established continuum mechanics framework. The main novelty concerns the specific application to graphene with the finite element implementation being straightforward when relying upon previous works on large deformation model for rubber-like materials. The series of virtual tests can be costly, but needs to be performed only once. Moreover, the developed model is fully capable to reproduce the linear elastic behaviour in small strain regime as well as the nonlinear that occurs in large strain regime.

The outline of the paper is as follows. We will address the problem of analysis of finite deformation of general, space-curved, elastic membranes in the next section. In the section 2 we present the virtual experiments performed on the SLGS and the development of the substitute continuum model in terms of principal stretches. In the section 3 we elaborate on the performance of the developed model, and give a closing remarks and future research in the section 5.

## 2. Continuum elastic membrane in finite deformations

### *2.1 Generalities and motivation*

We will first briefly revisit continuum model problem in large displacements and solution strategy. Let the position of each point be denoted with $\mathbf{X}$ and $\mathbf{x} = \boldsymbol{\varphi}(\mathbf{X})$ in reference ($\Omega$) and current ($\Omega^{\varphi}$) configuration, respectively, where $\boldsymbol{\varphi}(\mathbf{X})$ denotes the motion as a point transformation. For each point $\mathbf{X}$ we define the displacement vector $u(\mathbf{X}) = \mathbf{x} - \mathbf{X}$. When the SLGS is submitted to large deformations the difference between the initial configuration at the

beginning of the load program and the deformed configuration, can no longer be ignored as for the case of small deformations, characterized by small strain tensor, $\boldsymbol{\epsilon}$. There is a large variety (theoretically infinite) of possible choices for stress and strain tensors available for the continuum large strain problem formulation as presented in most of the textbooks covering the subject (see e.g., Ibrahimbegovic 2009, Wriggers 2008). For the continuum large strain problem the constitutive model formulation depends on the choice of the particular work-conjugate pair. Usually first Piola-Kirchhoff stress and deformation gradient ($\boldsymbol{P}$, $\boldsymbol{F}$) or second Piola-Kirchhoff stress and Green-Lagrange strain ($\boldsymbol{S}$, $\boldsymbol{E}$) are chosen to express internal work. We now construct the weak form of the continuum boundary value problem in $\Omega$ for the case of large displacements. This immediately introduces a solution strategy by weakening the way of satisfying the equilibrium, i.e. it is satisfied only in average sense. Therefore, we assume that Dirichlet boundary conditions $\mathbf{u} = \bar{\mathbf{u}}$ are prescribed on the part $\Gamma_{\mathrm{u}}$ of the boundary $\Gamma$. The nanostructure system treated as surrogate continuum is subjected to tractions $\bar{\mathbf{t}}$ on the part $\Gamma_{\sigma}$ of the boundary and to a volume forces $\mathbf{b}$ in $\Omega$. We choose a virtual displacement field $\mathbf{v}$ as infinitesimal and kinematically admissible with respect to Dirichlet boundary conditions, thus each component $v_i$ takes a zero value on the $\Gamma_{\mathrm{u}}$ i.e. $V_0 := \{v_i : \Omega \mapsto \mathbb{R} \,|\, [v_i]_{\Gamma_{u_i}} = 0\}$. We also suppose that the virtual displacement is supperposed on the deformed configuration and parameterized by the coordinates in the deformed configuration ($\Omega^{\varphi}$). For the real displacement vector field $\mathbf{u}$ the components ui are defined within $V := \{u_i : \Omega \mapsto \mathbb{R} \,|\, [u_i]_{\Gamma_{u_i}} = \bar{u}_i\}$. The weak form of equilibrium at large displacements in material description ($\Omega$) states

$$0 = G(\boldsymbol{\varphi}; \mathbf{v}) := \int_{\Omega} \boldsymbol{\Gamma} \cdot \mathbf{S} d\Omega - \int_{\Omega} \mathbf{v} \cdot \mathbf{b} d\Omega - \int_{\Gamma_{\sigma}} \mathbf{v} \cdot \bar{\mathbf{t}} d\Gamma, \tag{1}$$

where $\boldsymbol{\Gamma}$ is the virtual Green-Lagrange strain given as the directional derivative of the Green-Lagrange strain measure.

The constitutive model formulation depends on the choice of the particular work-conjugate pair, however the unique form of the constitutive relation can be written for the hyperelastic material model in terms of the strain energy potential, W(·). Energy potential is a unique choice, since all possibilities of the stress and strain measures are only different material representations of the same work. The generalised approach for establishing the well-posed form of the strain energy is given in terms of the polyconvexity conditions. The role of the polyconvexity conditions is to ensure that the large strain remains accompanied by large stress. Moreover, the polyconvexity conditions impose that the strain energy remains a convex function which can be written as

$$W(\alpha \mathbf{a}_1 + (1-\alpha)\mathbf{a}_2) \leq \alpha W(\mathbf{a}_1) + (1-\alpha) W(\mathbf{a}_2), \tag{2}$$

where $\mathbf{a}_1$ and $\mathbf{a}_2$ are functions representing certain intrinsic measure of deformation and $0 < \alpha < 1$. Besides the polyconvexity conditions applicable only to hyperelastic materials, there is a number of invariance restrictions on the general elastic response, which any constitutive model ought to respect. In order to describe the elastic response that satisfies the invariance requirements, the strain energy potential is usually expressed as a function of principal invariants

$$W(i_{1C}, i_{2C}, i_{3C}), \tag{3}$$

where the principal invariants of the right ($\boldsymbol{C} = \boldsymbol{F}^{\mathrm{T}}\boldsymbol{F}$) and left ($\boldsymbol{B} = \boldsymbol{F}\boldsymbol{F}^{\mathrm{T}}$) Cauchy-Green deformation tensors are given as

$$
\begin{aligned}
i_{1C} &:= \mathrm{tr}[\boldsymbol{F}^{\mathrm{T}}\boldsymbol{F}] \equiv \mathrm{tr}[\boldsymbol{F}\boldsymbol{F}^{\mathrm{T}}] =: i_{1B} \\
i_{2C} &:= \frac{1}{2}\left((\mathrm{tr}[\boldsymbol{C}])^2 - \mathrm{tr}[\boldsymbol{C}^2]\right) \equiv \frac{1}{2}\left((\mathrm{tr}[\boldsymbol{B}])^2 - \mathrm{tr}[\boldsymbol{B}^2]\right) =: i_{2B} \\
i_{3C} &:= \det[\boldsymbol{F}^{\mathrm{T}}\boldsymbol{F}] = (\det[\boldsymbol{F}])^2 \equiv \det[\boldsymbol{F}\boldsymbol{F}^{\mathrm{T}}] =: i_{3B}.
\end{aligned} \tag{4}
$$

### *2.2 Constitutive law in terms of principal stretches for large deformation of graphene*

An elegant alternative to (3) is the strain energy potential defined in terms of the principal stretches $\lambda_i$, $i$ = 1, 2, 3. These values correspond to the principal values of the stretch tensors, right $\boldsymbol{U}$ or left $\boldsymbol{V}$. This derives from the standard eigenvalue problem which can be written either in material (*a*) or in spatial (*b*) description

$$
(a)\quad (\boldsymbol{U} - \lambda_i \boldsymbol{I})\mathbf{n}_i = \mathbf{0}, \quad (b)\quad (\boldsymbol{V} - \lambda_i \boldsymbol{I}^{\boldsymbol{\varphi}})\mathbf{m}_i = \mathbf{0}. \tag{5}
$$

Note that the computed principal (eigen) values $\lambda_i$ from the Eq. (5) remain the same in both descriptions, but the corresponding eigenvectors $\mathbf{n}_i$ and $\mathbf{m}_i$ change. By solving these eigenvalue problems, we can obtain spectral decomposition of the deformation gradient, rotation tensor

$$
(a)\quad \boldsymbol{F} = \sum_{i=1}^{3} \lambda_i \mathbf{m}_i \otimes \mathbf{n}_i, \quad (b)\quad \boldsymbol{R} = \sum_{i=1}^{3} \mathbf{m}_i \otimes \mathbf{n}_i, \tag{6}
$$

and both stretch tensors

$$
(a)\quad \boldsymbol{U} = \sum_{i=1}^{3} \lambda_i \mathbf{n}_i \otimes \mathbf{n}_i, \quad (b)\quad \boldsymbol{V} = \sum_{i=1}^{3} \lambda_i \mathbf{m}_i \otimes \mathbf{m}_i. \tag{7}
$$

Note that these results hold for the principal vectors that form the ortho-normal principal frames, i.e., $\mathbf{n}_i \cdot \boldsymbol{I}\mathbf{n}_j = \delta_{ij}$, where $\delta_{ij}$ is the Kronecker delta. We further discuss the spectral decomposition of the Cauchy-Green tensors, related to the choice of the class of constitutive equations. Considering (6a) and its transpose

$$
\boldsymbol{F}^{\mathrm{T}} = \sum_{i=1}^{3} \lambda_i \mathbf{n}_i \otimes \mathbf{m}_i, \tag{8}
$$

the spectral decomposition for both Cauchy-Green tensors is given as

$$
(a)\quad \boldsymbol{C} = \sum_{i=1}^{3} \lambda_i^2 \mathbf{n}_i \otimes \mathbf{n}_i, \quad (b)\quad \boldsymbol{B} = \sum_{i=1}^{3} \lambda_i^2 \mathbf{m}_i \otimes \mathbf{m}_i. \tag{9}
$$

With these results in hand we can easily express the principal invariants from (4) in terms of the principal stretches

$$
i_{1C} := \lambda_1^2 + \lambda_2^2 + \lambda_3^2, \quad i_{2C} := \lambda_1^2\lambda_2^2 + \lambda_2^2\lambda_3^2 + \lambda_3^2\lambda_1^2, \quad i_{2C} := \lambda_1^2\lambda_2^2\lambda_3^2. \tag{10}
$$

Thus, any isotropic hyperelastic response that satisfies material invariance restriction can be expressed in terms of strain energy potential as a function of principal stretches. Thus, starting from the strain energy potential written as a function of principle invariants (3), we can express using (10) strain energy as a function of principal stretches

$$W(i_{1C}, i_{2C}, i_{3C}) \rightarrow W(\lambda_1, \lambda_2, \lambda_3). \tag{11}$$

For the elastic material behaviour the unit principal stretch corresponds to the case of no deformation which is accompanied by the zero value of strain energy

$$\lambda_i \rightarrow 1 \quad \Rightarrow \quad W(\lambda_i) \rightarrow 0. \tag{12}$$

Formulating the strain energy potential as in (11) makes it simple to check the polyconvexity conditions described above. These conditions enforce that large stresses should accompany large values of strains which is written in terms of principal stretches as

$$\begin{aligned} W(\lambda_i) &\rightarrow \infty \qquad \text{if } \{\lambda_1, \lambda_2, \lambda_3\} \rightarrow \infty \quad \text{(in tension)}, \\ W(\lambda_i) &\rightarrow \infty \qquad \text{if } \{\lambda_1, \lambda_2, \lambda_3\} \rightarrow 0^+ \quad \text{(in compression)}. \end{aligned} \tag{13}$$

The last result states that polyconvexity conditions require the strain energy convexity with respect to each principal stretch. Non-convexity is responsible for many phenomena like the development of dislocations and phase changes, however we are not dealing with these issues in this work.

We turn now to 2D case formulation that describes the SLGS sheet. Thus, putting graphene sheet in the plane $x_1x_2$, we are neglecting the out of plane stretch $\lambda_3$, following the usual hypothesis for the membrane theory. Since the sheet is made of a single atomic layer and the out-of-plane strains and stresses might be difficult to interpret, we restrict the considerations to the in-plane 2D continuum mechanics (this assumption is made by majority of authors dealing with graphene, see e.g., Volokh, (2012)). Considering the mentioned assumption the strain energy density (SED) in (11) becomes $W(\lambda_1, \lambda_2)$. We further present the procedure to calculate second Piola-Kirchhoff stress ($\boldsymbol{S}$) and tangent elasticity ($\mathbb{C}$) tensors from the strain potential written in terms of the principal stretches. This computation is still performed in the conventional manner as

$$(a) \quad \boldsymbol{S} = \frac{\partial W}{\partial \boldsymbol{E}} = 2\frac{\partial W}{\partial \boldsymbol{C}}, \quad (b)\ \mathbb{C} = \frac{\partial \boldsymbol{S}}{\partial \boldsymbol{E}} = 2\frac{\partial \boldsymbol{S}}{\partial \boldsymbol{C}}. \tag{14}$$

However, the computation of the stress and tangent elasticity tensors from the material model given by $W(\lambda_1, \lambda_2)$ is not performed directly, but rather using a simple chain rule. Thus, an important role is played by the auxiliary result pertaining to change of the principal stretch $\lambda_i$ with respect to the change of the deformation. This result can be obtained by applying the Gateaux derivative formalism to the corresponding eigenvalue problem leading to

$$\frac{\partial \lambda_i}{\partial \boldsymbol{C}} = \frac{1}{2\lambda_i} \mathbf{n}_i \otimes \mathbf{n}_i. \tag{15}$$

With this result in hand, we can calculate the second Piola-Kirchhoff stress tensor from the SED potential written in terms of principal stretches

$$\boldsymbol{S} = \sum_{i=1}^{2} \frac{1}{\lambda_i} \frac{\partial W(\lambda_1, \lambda_2)}{\partial \lambda_i} \mathbf{n}_i \otimes \mathbf{n}_i. \tag{16}$$

Comparing Eqs. (16) and (9(a)) one can notice that the second Piola-Kirchhoff stress tensor is coaxial with the right Cauchy-Green tensor. Existence of the coaxial energy-conjugate pair enables the solution of the problem of finite deformation membrane relaying on the Cartesian structure. The second Piola-Kirchhoff stress tensor can be further decomposed as

$$\boldsymbol{S} = \sum_{i=1}^{2} s_i \mathbf{n}_i \otimes \mathbf{n}_i, \tag{17}$$

where $\mathbf{n}_i$ represents the same eigenvectors as in (9(a)), and the term $s_i$ denotes the principal stresses which can be written as

$$s_i = \frac{1}{\lambda_i} \frac{\partial W(\lambda_1, \lambda_2)}{\partial \lambda_i}. \tag{18}$$

Next, we turn to the calculation of the elastic tangent modulus. This is done in the same manner, i.e., by performing a next step of directional derivative computation, which gives

$$\mathbb{C} = 2 \sum_{i=1}^{2} \frac{\partial s_i}{\partial \boldsymbol{C}} \mathbf{n}_i \otimes \mathbf{n}_i + 2 \sum_{i=1}^{2} s_i \frac{\partial}{\partial \boldsymbol{C}} (\mathbf{n}_i \otimes \mathbf{n}_i). \tag{19}$$

The first and the second terms on the right hand side in (19) correspond to material ($\mathbb{C}_{mat}$) and geometric ($\mathbb{C}_{geo}$) part of the tangent elasticity tensor, respectively. Using the auxiliary result in (15) we obtain the expression for the material part of the tangent elasticity tensor

$$\mathbb{C}_{mat} = \sum_{i=1}^{2} \sum_{j=1}^{2} \underbrace{\left( \frac{1}{\lambda_j} \frac{\partial s_i}{\partial \lambda_j} \right)}_{D_{ij}} [\mathbf{n}_i \otimes \mathbf{n}_i][\mathbf{n}_j \otimes \mathbf{n}_j]. \tag{20}$$

Note that the material part of the tangent elasticity tensor is usually given in terms of its reduced form $D_{ij}$ in principal axes; see Ibrahimbegovic and Gruttmann (1993). The derivation of explicit form of the geometric part of the tangent elasticity tensor starts from the spectral decomposition of the right Cauchy-Green strain tensor (9) and considers a systematic usage of the auxiliary result in (15). Due to brevity we omitted this derivation and we give the final expression of the elastic tangent modulus in tensor notation

$$\mathbb{C} := \sum_{i=1}^{2} \sum_{j=1}^{2} D_{ij} [\mathbf{n}_i \otimes \mathbf{n}_i][\mathbf{n}_j \otimes \mathbf{n}_j] + 2 \frac{s_1 - s_2}{\lambda_1^2 - \lambda_2^2} \left[ \mathcal{I} - (\mathbf{n}_1 \otimes \mathbf{n}_1) \otimes (\mathbf{n}_1 \otimes \mathbf{n}_1) - (\mathbf{n}_2 \otimes \mathbf{n}_2) \otimes (\mathbf{n}_2 \otimes \mathbf{n}_2) \right], \tag{21}$$

where $\mathcal{I} = \frac{1}{2}(\delta_{ik}\delta_{jl} + \delta_{il}\delta_{jk})$.

The constitutive law in terms of principal stretches for large deformation of membrane (used here for the SLGS), namely the expression (18) and (21), are used directly in the finite element solution procedure. The details about the 2D elastic membrane finite element can be found in most of the books dealing with nonlinear solid mechanics, and will not be discussed herein. For the completeness, we summarize the main steps needed in the finite element approximation, which for the presented constitutive law in terms of principal stretches boils down simply to the matrix form of the results obtained for principal stresses and elasticity, see Appendix A.

## 3. Development of constitutive law from virtual experiments on molecular model of graphene

### *3.1 Molecular model*

In Section 2, a continuum model problem in large displacements is presented. Likewise, we introduce here briefly the molecular model problem. We consider a reference domain $\Omega_a \in \mathbb{R}^3$ which is occupied by $N$ atoms placed within graphene nanostructure. A major feature of the structure of graphene is the hexagon pattern that repeats itself periodically in space. As a result of the periodicity, each atom is bonded to three neighbouring atoms. Such structure is mainly due to the process of $sp^2$ hybridization during which one $s$−orbital and two $p$−orbitals combine to form three hybrid $sp^2$−orbitals at 120° to each other within a plane Atkins and De Paula (2006), Ruoff *et al.* (2003). This covalent bond, often referred to as the $\sigma$−bond, is a strong chemical bond and plays an important role in the impressive mechanical properties of graphene, while the out-of-plane bond (the $\pi$−bond) that is relatively weak contributes to the interaction between the layers of graphene.

Let $\mathbf{X}_i$ and $\mathbf{x}_i$ denote, respectively, the position vectors in the reference and the current configurations of atom $i$, where $i = 1, \ldots, N$. The corresponding displacement vector of atom $i$ is given by $\mathbf{d}_i = \mathbf{x}_i - \mathbf{X}_i$. The boundary conditions are imposed atom-wise in a quasi-static manner, such that either the displacement $\bar{\mathbf{d}}_i$ or the external point force $\mathbf{f}_i$ is given. The total energy ($E_{tot}$) stored in the atomic structure is given by

$$E_{tot} = U(\mathbf{x}_1, \ldots, \mathbf{x}_N) - \sum_i^N \bar{\mathbf{f}}_i \cdot \mathbf{d}_i, \tag{22}$$

where $U$ denotes the energy stored in the atomic bonds, as presented in sequel, and the second term on the right-hand side represents the external energy. The state of equilibrium of the atomistic system requires the variation of the total energy to be equal to zero

$$\delta E_{tot} = \sum_i^N \left( \frac{\partial U}{\partial \mathbf{x}_i} - \bar{\mathbf{f}}_i \right) \cdot \delta \mathbf{x}_i = 0, \tag{23}$$

where $\delta \mathbf{x}_i$ represents the kinematically admissible virtual motion. Linearizing (23) and writing the result in matrix notation leads to

$$\mathbf{K}^{(k)} \Delta \mathbf{d}^{(k)} = \mathbf{F}^{(k)}, \tag{24}$$

where $\Delta \mathbf{d}^{(k)}$ is the displacement increment corresponding to the $k$-th load increment, whereas $\mathbf{K}^{(k)}$ and $\mathbf{F}^{(k)}$ are global stiffness and the residual vector, respectively. The latter can explicitly be defined as

$$\mathbf{K}_{ij} = \frac{\partial^2 U}{\partial \mathbf{x}_i \partial \mathbf{x}_j}, \qquad \mathbf{F}_i = \frac{\partial U}{\partial \mathbf{x}_i} - \bar{\mathbf{f}}_i. \tag{25}$$

Unlike conventional FE method for continuum mechanics, we derive and assemble the stiffness and residual matrices by looping over all atoms. Due to the non-linear nature of the interatomic potentials and geometrically nonlinear kinematics, an incremental-iterative solver is used. For each load increment, several Newton iterations are performed, until convergence criteria are met. After each iteration ($k$) the atomic positions are updated as

$$\mathbf{x}_i^{(k+1)} = \mathbf{x}_i^{(k)} + \Delta \mathbf{d}^{(k)}. \tag{26}$$

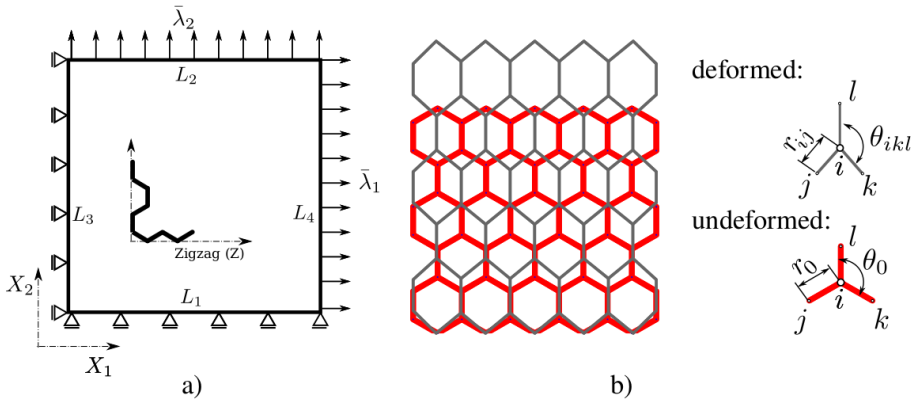


Fig. 1 Scheme of the lattice sample with symmetry BCs used for biaxial tensile tests a). The envelope of the sample is composed of lines $L_1$ to $L_4$ which coincides with boundary atoms. The overlay plot of the undeformed (red) and deformed (grey) shapes of the small graphene lattice sample for the case $\bar{\lambda}_1 = 1, \bar{\lambda}_2 = 1.15$ b). A zoom on the bulk atom $i$ is shown with the bond length and angle given in the undeformed ($r_0$, $\theta_0$) and deformed ($r_{ij}$, $\theta_{ikl}$) configurations

The initial iteration $k = 0$ starts at the initial configuration of the atomic system, with the position vector, $\mathbf{x}_i^{(0)} = \mathbf{X}_i$.

Looking at the Eq. (25) it is obvious that the heart of molecular model lays in the internal energy governed by the interatomic potential. For the molecular simulation of a graphene sheet, a Morse potential Morse (1929) is used, more precisely we use its modified version following Belytschko *et al*. (2002). The modified Morse potential is a sum of pair and angular parts given as

$$U = \sum_{\text{bonds}} V_p^M(r) + \sum_{\text{angles}} V_\theta^M(\theta). \tag{27}$$

The first term is a function of the chosen atom distance $r$ to its first neighbour, whereas the second depends upon angle $\theta$ between particular atom bonds (see Fig. 1 (b)) in sequel). For the modified Morse potential, the bond energy terms are given as

$$V_p^M(r) = D_e \left[ (1 - e^{-\beta(r - r_0)})^2 - 1 \right], \tag{28}$$

$$V_\theta^M(\theta) = \frac{1}{2} k_\theta (\theta - \theta_0)^2 [1 + k_{sext}(\theta - \theta_0)^4], \tag{29}$$

where the constants of the potential according to Belytschko *et al*. (2002) are: $D_e = 6.03105 \times 10^{-19}$ Nm, $\beta = 2.625 \times 10^{10} \text{m}^{-1}$, $k_\theta = 0.9 \times 10^{-18}$ Nm rad$^{-2}$, $k_{sext} = 0.754$ rad$^{-4}$, the initial value of the bond length $r_0 = 1.39 \times 10^{-10}$ m and the bond angle $\theta_0 = 2\pi/3$ rad. The numerical implementation of MM model based on modified Morse potential, i.e., the forming of the residual force and tangent stiffness matrices, and the assembly procedure are given in more detail in Marenić *et al*. (2013). A general procedure for carbon structures is shown in Wackerfuss (2009), where the molecular model is plugged within the formalism of the finite element method.

### 3.2 Virtual experiments on representative lattice

We show subsequently the biaxial tensile tests performed on the graphene lattice sample using the presented molecular model implemented in the inhouse MATLAB code. The scheme of the representative lattice element with the symmetry boundary conditions is illustrated in Fig. 1 (a). The square envelope representing the boundary of the graphene sheet is composed of lines $L_1$ to $L_4$. Atoms which are on the lower and left lines $L_1$ and $L_3$ of the sample are pinned with $u_2 = 0$ and $u_1 = 0$, respectively. The boundary atoms which belong to the upper and right lines, $L_1$ and $L_4$, have a given displacement to produce the stretch $\bar{\lambda}$. Overlay plot of the undeformed and deformed lattice sample is shown in Fig. 1 (b) for the case where $\bar{\lambda}_1 = 1$ and $\bar{\lambda}_2 = 1.15$ (deformed shape is given with scale factor, and really small lattice sample is shown due to visibility). Geometrical potential parameters related to the initial, undeformed geometry of the lattice ($r_0$, $\theta_0$) are shown in the zoom on the bulk atom $i$. Given deformation maps the atom $i$ and his neighborhood to deformed configuration ($r_0 \to r_{ij}, \theta_0 \to \theta_{ikl}$), as schematically shown on the right of Fig. 1 (b).

### 3.3 Equivalent continuum

In order to construct equivalent continuum potential $W_{fit}(\lambda_1, \lambda_2)$ we determine the equilibrium potential energy of atomistic system. Note that the boundary atoms have two neighboring atoms instead of three for the bulk ones (on the right side of Fig. 1 (b)) bulk atom *i* together with its neighbors *j*, *k*, *l* is shown). Thus, the equilibrium energy density of the finite size lattice sample depends on the ratio of boundary and bulk atoms. The smaller the ratio the smaller is the number of the boundary with respect to bulk atoms, and the energy density converges to the infinite lattice (where all atoms have full neighborhood). This convergence tendency is visible, e.g., on Fig. 10 (b)) in Marenić *et al*. (2013). Our approach which considers the development of the surrogate continuum model based on the virtual test on representative graphene samples works well for both really small and/or narrow lattice (e.g., graphene nano-ribbons Xu (2009) for nano-electro-mechanical systems) as well as for the larger ones. We compute the equilibrium potential energy of atomistic system for the series of loading cases. These loading cases are designed to form the uniform grid in the space of $\lambda_1, \lambda_2$ in the range

$$\lambda_1 = \{1, \ldots, \bar{\lambda}\}, \quad \lambda_2 = \{1, \ldots, \bar{\lambda}\}, \tag{30}$$

resulting with the cloud of points $W(\lambda_1, \lambda_2)$, shown as dots in Fig. 2. Note that in the above equation the given values of stretch $\bar{\lambda} \geq 1$, which corresponds only to in-plane tension. The compressive stresses even the ones transmitted by the substrate causes out of plane buckling of the SLGS, see Zhang and Arroyo (2013), which is not considered in this work. The energy distribution for the series of loading cases is further used to perform a least squares, polynomial surface fitting (see Fig. 2) with SED potential given as

$$W_{\text{fit}}(\lambda_1, \lambda_2) = \sum_{i}^{n} \sum_{j}^{n} a_{ij} \lambda_1^i \lambda_2^j, \tag{31}$$

where *i* and *j* are the degree in $\lambda_1$ and in $\lambda_2$, respectively. The total degree of the polynomial is the maximum of *i* and *j*. Note that the total degree of the polynomial cannot exceed the maximum of *i* and *j*. Hence if $i = j = 5$, for instance, the coefficients $a_{ij} = 0$ if $i + j > 5$. As mentioned above for the initial iteration we have $\mathbf{x}_i^{(0)} = \mathbf{X}_i$, that is the $r = r_0$ and $\theta = \theta_0$, and

considering our choice of the modified Morse potential and Eqs. (28) and (29), the value of SED turns to be zero for the unit stretch. No other constraints were introduced in the model fit.

Using fitted, polynomial potential (31), and following the Eqs. (16) to (18) we can calculate the stress components. We present in Fig. 3 surface plots (closed form, polynomials obtained by energy fit) of the nonzero stress components. Note that stress components are conveniently written in terms of the stress vector, as shown in appendix A. In addition, using spectral decomposition (17 ) one computes directly principal stresses using (18). In our consideration, this further simplifies stress vector to two components. Knowing principal stresses and directions, finite element implementation further relays to the internal force vector, and tangent elasticity matrix computation. Stress vector (in terms of principal stresses) is directly plugged into membrane finite element equations, for details see appendix, Eqs. (37) and (38).

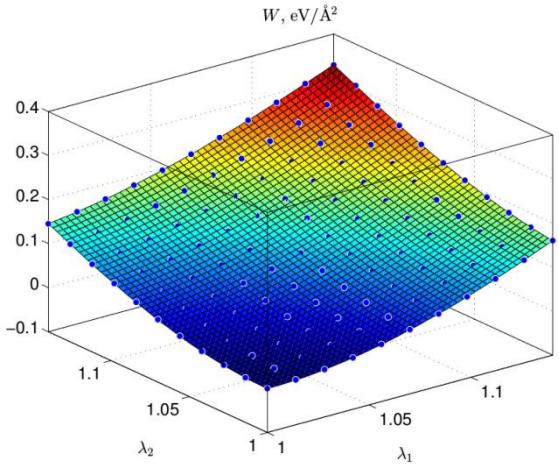


Fig. 2 The surface plot of the strain energy density polynomial surface fit $W_{fit}(\lambda_1, \lambda_2)$. The fit is obtained by means of series of biaxial tests performed by molecular mechanics simulation ($\widehat{W}(\lambda_1, \lambda_2)$) represented with circular markers on the grid $0 \leq \bar{\lambda}_i \leq 1.15$, $i = 1, 2$

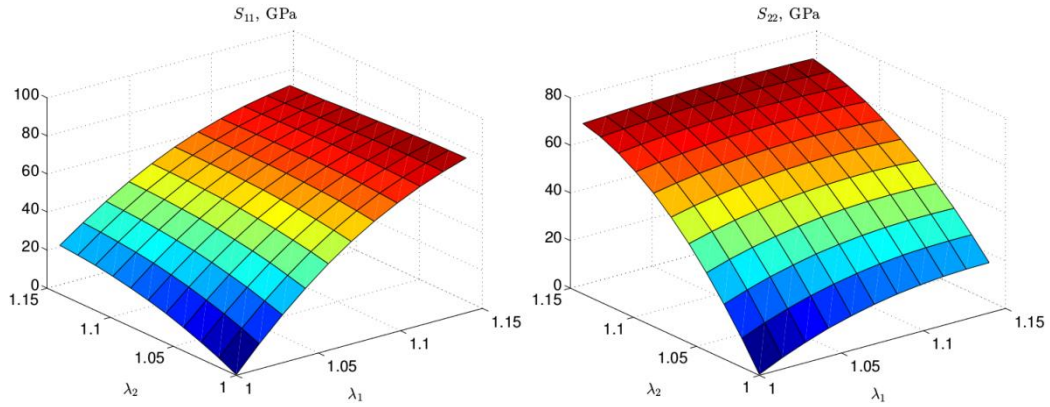


Fig. 3 Surface plot of the nonzero stress components vs. principal stretches.

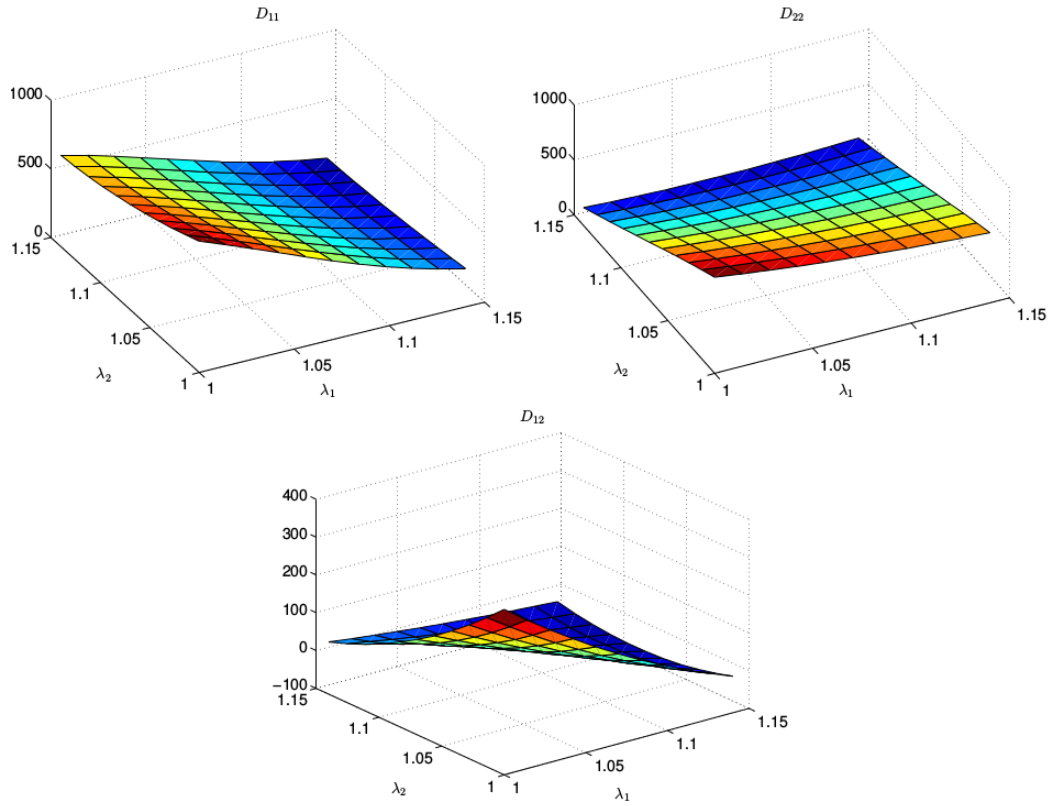


Fig. 4 Surface plot of the components of reduced tangent elastic modulus. The values are given in GPa.

From the plots in Fig. 3 we can note that the maximum stress does not correspond to the maximum biaxial stretches, that is, to the case when $\lambda_i = \bar{\lambda}$. This phenomena is related to the given hexagonal lattice structure, chosen interatomic potential, as well as the finite deformation regime and will be further analyzed and explained in sequel.

Analogously to the stress, using fitted potential and following (20) we present the surface plots of the components of material part of the tangent elasticity tensor using its reduced form $D_{ij}$, on the Fig. 4, with $D_{12} = D_{21}$ due to symmetry.

## 4. Analysis and verification of the constitutive model

We seek first to explain the effect illustrated in Fig. 3, related to the fact that the stress is not maximum for the maximum biaxial stretch. Thus, we present a variation of the stress component $S_{11}$ with $\lambda_1$, taking the prestretch in the perpendicular direction ($\lambda_2$) as a parameter, see left plot on the Fig. 5. We can observe that for larger deformation (roughly $\lambda_1 > 10\%$), value of the $S_{11}$ decreases for higher pre-stretch ($\lambda_2$). We can also note this effect by plotting $S_{11}$ vs. $\lambda_2$ with the

parameter $\lambda_1$, as depicted in the right plot in the Figure 5, where we clearly see the decrease of $S_{11}$ with evolving stretch in direction 2, for higher pre-stretch in direction 1. Needless to say, this effect is fully captured in the developed homogenised, continuum model, i.e., the stress decrease is noticeable in terms of the tangent elastic modulus. Namely, the component $D_{12}$ of the tangent elastic modulus (shown on the bottom plot in Fig. 4) which governs the relation between $S_{11}$ and strain in direction 2, becomes negative for large deformation. An analogous effect can be seen for the stress component $S_{22}$, thus these plots are not shown.

In order to further explain this effect of stress decrease, we turn to the study of the nanostructure of graphene. Moreover, we imposed biaxial, so-called half snail loading program depicted in Fig. 6 (a) and we trace the corresponding lattice deformation. Given loading program considers stretching in the first half of the loading time in direction 2 (up to $\lambda_2 = \lambda_{2,max}$) while holding the lattice sample with $\lambda_1 = 1$. Second half of the loading program considers holding the stretch $\lambda_2 = \lambda_{2,max}$ while loading in direction 1. Note that the stretches we did in our virtual experiments did not go more than about 15% in each principal direction. This value is related to the chosen interatomic potential, more precisely to its pair part. Namely, the derivative of the pair part (28) with respect to the pair bond separation $r$ gives a pair force $F_p(r)$. This function has a peak value after which the force diminishes with further bond separation. There are two reasons why we are not taking this in our consideration. The first one pertains to the choice of interatomic potential which is not suitable for the bond fracture modeling. The second is related to the implemented Newton iterative algorithm which is not suitable when the effect similar to material softening occurs. During the loading program we follow the deformation in C−C bonds by selecting the bulk atom *i* and his neighbours *j* and *k* (see Fig. 6(b))), omitting *l* due to symmetry. We note that the choice of the atom we trace is free, given that it is far enough from the boundary. The bond separation ($\Delta r$) evolving with the loading (given as pseudo-time) is shown on Fig. 6(c)).

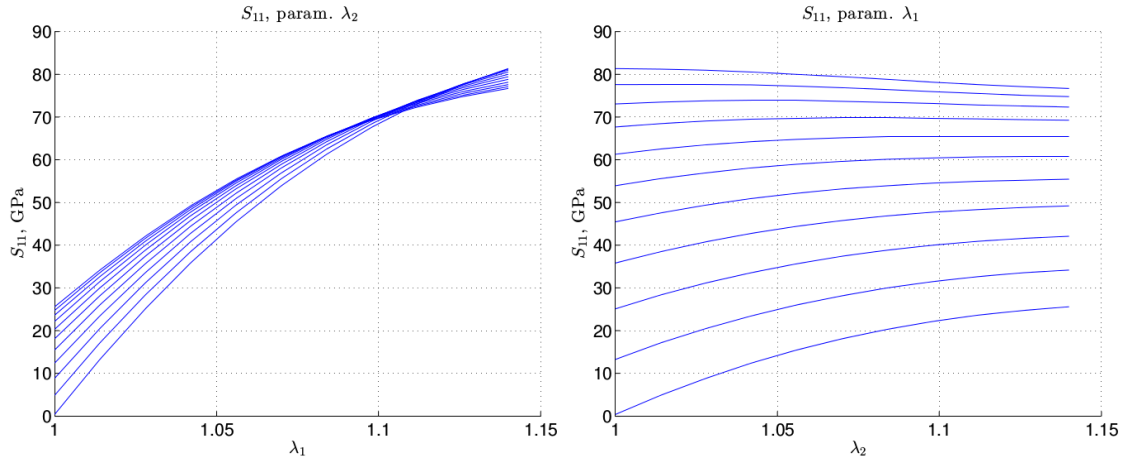


Fig. 5 The stress-stretch plots showing the component $S_{11}$ versus: stretch $\lambda_1$ with parameter $\lambda_2$ (left plot), and stretch $\lambda_2$ with parameter $\lambda_1$ (right plot). The parameter is in the range $\lambda_i = 1,...,\bar{\lambda}$, where the lower-most stress curve corresponds to the value of the paremeter $\lambda_i = 1$, while the upper-most corresponds to $\lambda_i = \bar{\lambda}$

We observe that for the first half of the load program with stretch in direction 2, both $\Delta r_{ij}$ and $\Delta r_{ik}$ are increasing. However, in the second part of the load program the bond separation $\Delta r_{ij}$ passes a peak value. This effect is related to the interplay of the pair and angular parts of the used modified Morse potential, as well as to the geometric nonlinearity, i.e., the large rotations of the bonds. The latter is causing the influence of the angular term of the modified Morse potential (29) to overcome the influence of the pair part (given in (28)). Finally, this causes the global response of the nanostructure defined in terms of stress-stretch diagram to show the stress decrease in large deformation regime which is noticed in the developed continuum model.

Next, in Fig. 7 we show the cross-sections from the Fig. 4 (similarly like it was done for the stresses in Fig. 5). This gives the evolution of the components of reduced tangent elastic modulus. Namely, we show $D_{11}$ versus $\lambda_1$ with the pre-stretch $\lambda_2$ as a parameter, and likewise, $D_{22}$ versus $\lambda_2$ with the parameter $\lambda_1$. The thick lines with markers (in Fig. 7) denote the evolution of $D_{ii}$ without pre-stretch. That is, dashed line with circular markers represents the $D_{11}(\lambda_1)$ for $\lambda_2 = 1$. Analogously, full line with square markers shows $D_{22}(\lambda_2)$ for $\lambda_1 = 1$. Any material description of an elastic constitutive law for large deformations should reduce to Hooke's law for the case of small deformation. Thus we proceed with the constitutive model verification using results from the literature. We perform this verification by comparison with the limiting case of small deformations considered in Marenić *et al*. (2013). The numerical values of the initial stiffness obtained from the fitted continuum model are as follows

$$\begin{aligned} D_{11}|_{\lambda_i=1} &= 956.95\text{GPa}, \\ D_{22}|_{\lambda_i=1} &= 876.35\text{GPa}. \end{aligned} \tag{32}$$

We note that this corresponds to the results presented in Marenić *et al*. (2013) considering the case $E_{|V'}$. Moreover, plotting the evolution of the components of reduced tangent elastic modulus with the increasing (corresponding) pre-stretch we end up with a band which is depicted for the whole range $\lambda_i = 1 \ldots \bar{\lambda}$ in Fig. 7. We note also that the increase of the pre-stretch causes the decrease of stiffness.

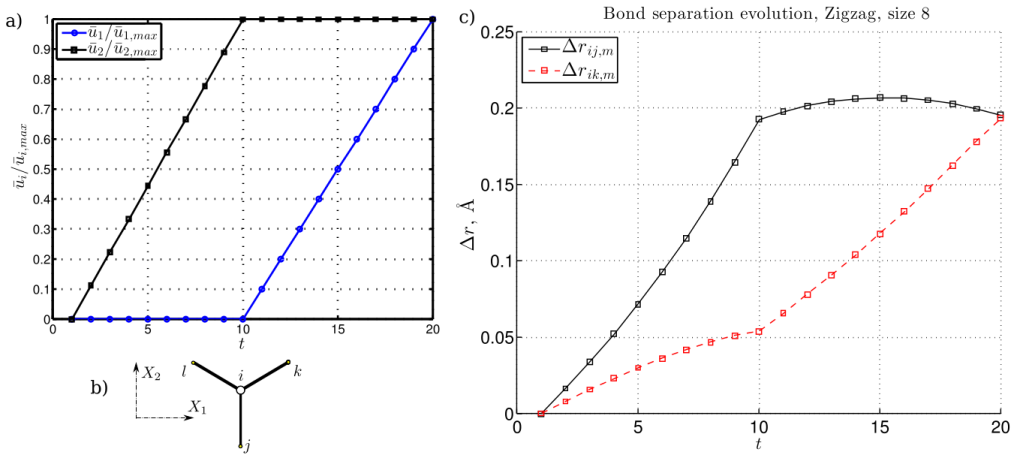


Fig. 6 Load program showing the given displacements (upper and right edges) with respect to the pseudo time (a), and (b) the bulk atom $i$ with its neighbourhood. The given load program causes the lattice deformation as presented in (c). Due to symmetry, the bond separation $\Delta r_{il}$ is equal as $\Delta r_{ij}$, and is thus omitted

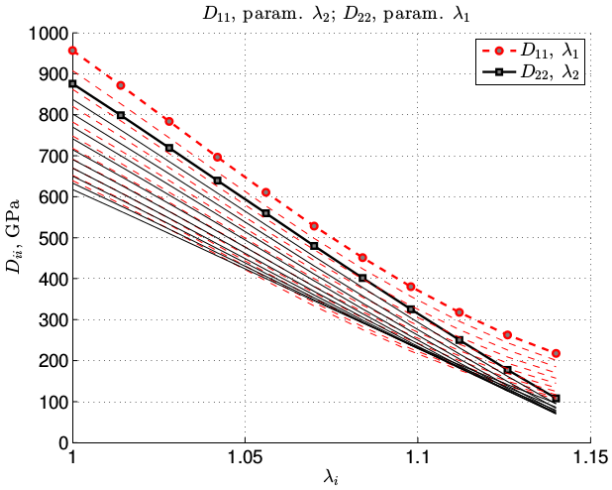


Fig. 7 Evolution of the diagonal components of the reduced tangent elastic modulus with the associated stretches. The thick lines with markers denote the evolution of $D_{ii}$ without pre-stretch

## 5. Conclusions

We have shown the continuum formulation of the in plane behaviour of graphene based on the hyperelastic potential given in terms of the principal stretches. The developed model is based on the well-established continuum mechanics framework, and fully capable to reproduce the linear elastic behaviour in small strain regime as well as the stress release caused by intrinsic geometric non-linearity of the interatomic bonds that occurs in large strain regime. Moreover, this formulation fits perfectly to the finite element implementation of the elastic membranes based on the Cartesian structure, i.e., co-axial energy-conjugate pairs of stress and strain.

The procedure performed here concerns virtual experiments performed on the graphene samples. Thus, this approach should work for lattices of other two-dimensional materials like e.g. boron nitride Novoselov *et al.* (2005), Topsakal and Ciraci (2010) which may have more complex lattice. The latter yields at the bottom line more complicated deformation mechanism on the lattice level and may preclude the Cauchy-Born rule, as a common link between atomistic and continuum scales, to be valid. Thus we plan to confront our large strain surrogate continuum model based on the numerical homogenization procedure with the Cauchy-Born based approach. In addition, we presented here only the modeling of the in plane large deformation of single layer graphene sheet, however, the extension to axisymmetric (like the Carbon Nano Tube) or arbitrary curved membrane is possible (see e.g. Ibrahimbegovic 1994), and will be concerned in future research.

## Acknowledgments

This work was supported by Labex MS2T post-doctoral fellowship.

## References


Abraham, R. and Marsden, J. E. (1987), *Foundations of mechanics*, Addison-Wesley.

Arroyo, M. and Belytschko, T. (2002), "An atomistic-based finite deformation membrane for single layer crystalline films", *J. Mech. Phys. Solids*, **50**(9), 1941-1977.

Atkins, P. and De Paula, J. (2006), Physical Chemistry, Oxford University Press, 8rev ed edition.

Belytschko, T., Liu, W. K. and Moran, B. (2000), Nonlinear Finite Elements for Continua and Structures. Wiley.

Belytschko, T., Xiao, S.P., Schatz, G.C. and Ruoff, R.S. (2002), "Atomistic simulations of nanotube fracture", *Phys. Rev. B*, **65**(23), 235430.

Brenner, D.W. (1990), "Empirical potential for hydrocarbons for use in simulating the chemical vapor deposition of diamond films", *Phys. Rev. B*, **42**, 9458-9471.

Brenner, D.W., Shenderova, O.A., Harrison, J.A., Stuart, S.J., Ni, B. and Sinnott, S.B. (2002), "A second-generation reactive empirical bond order (rebo) potential energy expression for hydrocarbons", *J. Phys.: Condensed Matter*, **14**(4), 783.

Bedoui, F. and Cauvin, L. (2012), "Elastic properties prediction of nano-clay re- inforced polymers using hybrid micromechanical models", *Comput. Mater. Sci.*, **65**, 309-314.

Cadelano, E., Palla, P.L., Giordano, S. and Colombo, L. (2009), "Nonlinear elasticity of monolayer grapheme", *Phys. Rev. Lett.*, **102**, 235502.

Caillerie, D., Mourat, A. and Raoult, A. (2006), "Discrete homogenization in graphene sheet modeling", *J. Elasticity*, **84**, 33-68.

Ericksen, J. (2008), "On the cauchyborn rule", *Math. Mech.Solids*, **13**, 199-220.

Ericksen, J.L. (1984), "The cauchy and born hypotheses for crystals. Phase transformation and material instabilities in solids" - from book 'Mechanics and Mathematics of Crystals: Selected Papers of J. L. Ericksen' by Millard F. Beatty and Michael A. Hayes, page 6177.

Geim, A.K. and Novoselov, K.S. (2007), "The rise of grapheme", *Nature Mater.*, **6**, 183-191.

Gelineau, P., Stepie, M., Weigand, S., Cauvin, L. and Bdoui, F. (2015), "Elastic properties prediction of nano-clay reinforced polymer using multi-scale modeling based on a multi-scale characterization", *Mech. Mater.*, **89**, 12- 22.

Georgantzinos, S., Giannopoulos, G. and Anifantis, N. (2010), "Numerical investigation of elastic mechanical properties of graphene structures", *Mater. Des.*, **31**(10), 4646 -4654.

Gmez, H., Ram, M.K., Alvi, F., Villalba, P., Stefanakos, E.L. and Kumar, A. (2011), "Graphene-conducting polymer nanocomposite as novel electrode for supercapacitors", *J. Power Sources*, **196**(8), 4102 -4108.

Hu, K., Kulkarni, D.D., Choi, I. and Tsukruk, V.V. (2014), "Graphene-polymer nanocom- posites for structural and functional applications", *Progress in Polymer Sci.*, **39**(11), 1934- 1972.

Huang, Y., Wu, J. and Hwang, K.C. (2006), "Thickness of graphene and single-wall carbon nanotubes", *Phys. Rev. B*, **74**, 245413.

Huet, C. (1990), "Application of variational concepts to size effects in elastic heterogeneous bodies", *J. Mech. Phys. Solids*, **38**(6), 813- 841.

Ibrahimbegovic, A. (1994), "Finite elastoplastic deformations of space-curved membranes", *Comput. Method. Appl. M.*, **119**, 371-394.

Ibrahimbegovic, A. (2009), *Nonlinear Solid Mechanics*, Springer.

Ibrahimbegovic, A. and Gruttmann, F. (1993), "A consistent finite element formulation of nonlinear membrane shell theory with particular reference to elastic rubberlike material", *Finite Elem. Anal. Des.*, **12**, 75-86.

Lee, C., Wei, X., Kysar, J. and Hone, J. (2008), "Measurement of the elastic properties and intrinsic strength of monolayer graphene", *Science*, **321**(5887), 385-388.

Lu, Q., Gao, W. and Huang, R. (2011), "Atomistic simulation and continuum modeling of graphene nanoribbons under uniaxial tension", *Model. Simul. Mater. Sc.*, **19**(5), 054006.

Lu, Q. and Huang, R. (2009), "Nonlinear mechanics of single-atomic-layer grephene sheets", *Int. J. Appl.*

*Mech.*, **1**, 443-467.
Marenić, E., Ibrahimbegovic, A., Soric, J. and Guidault, P.A. (2013), "Homogenized elastic properties of graphene for small deformations", *Materials: Special Issue "Computational Modeling and Simulation in Materials Study"*, **6**(9), 3764-3782.
Markovic, D. and Ibrahimbegovic, A. (2004), "On micro-macro inter- face conditions for micro scale based FEM for inelastic behavior of heterogeneous materials", *Comput. Method. Appl. M.*, **193**(48-51), 5503-5523.
Morse, P.M. (1929), "Diatomic molecules according to the wave mechanics. ii. vibrational levels", *Phys. Rev.*, **34**, 57-64.
Novoselov, K.S., Jiang, D., Schedin, F., Booth, T.J., Khotkevich, V.V., Morozov, S.V. and Geim, A.K. (2005), "Two-dimensional atomic crystals", *PNAS*, **102**-30, 10451-10453.
Reddy, C.D., Rajendran, S. and Liew, K.M. (2006), "Equilibrium configuration and continuum elastic properties of finite sized grapheme", *Nanotechnology*, **17**(3), 864.
Ruoff, R.S., Qian, D. and Liu, W.K. (2003), "Mechanical properties of carbon nanotubes: theoretical predictions and experimental measurements", *Comptes Rendus Physique*, **4**(9), 993-1008.
Singh, V., Joung, D., Zhai, L., Das, S., Khondaker, S.I. and Seal, S. (2011), "Graphene based materials: Past, present and future", *Prog. Mater. Sci.*, **56**(8), 1178 -1271.
Stankovich, S., Dikin, D.A., Dommett, G.H.B., Kohlhaas, K.M., Zimney, E.J., Stach, E.A., Piner, R.D., Nguyen, S.T. and Ruoff, R.S. (2006), "Graphene-based composite materials", *Nature*, **442**(7100), 282-286.
Tersoff, J. (1986), "New empirical model for the structural properties of silicon", *Phys. Rev. Lett.*, **56**, 632-635.
Topsakal, M. and Ciraci, S. (2010), "Elastic and plastic deformation of graphene, silicene, and boron nitride honeycomb nanoribbons under uniaxial tension: A first-principles density- functional theory study", *Phys. Rev. B*, **81**, 024107.
Volokh, K. (2012), "On the strength of grapheme", *J. Appl. Mech.- T ASME*, **79**, 064501- 5.
Wackerfuss, J. (2009), "Molecular mechanics in the context of the finite element method", *Int. J. Numer. Mett. Eng.*, **77**, 969-997.
Wriggers, P. (2008), *Nonlinear Finite Element Methods*, Springer.
Xu, Z. (2009), "Graphene nano-ribbons under tension", *Journal of Computational and Theoretical Nanoscience*, **6**, 625-628.
Zanzotto, G. (1996), "The cauchy-born hypothesis, nonlinear elasticity and mechanical twining in crystals", *Acta Crystallographica*, **52**, 839-849.
Zhang, K. and Arroyo, M. (2013), "Adhesion and friction control localized folding in supported grapheme", *J. Appl. Phys.*, **113**, 193501-8.
Zhao, H., Min, K. and Aluru, N.. (2009), "Size and chirality dependent elastic properties of graphene nanoribbons under uniaxial tension", *Nanoletters*, **9-8**, 3012-3015.

## Appendix Finite element implementation

The details about the 2D plane elastic membrane finite element can be found in most of the books dealing with nonlinear solid mechanics e.g., Ibrahimbegovic (2009), Wriggers (2008), Belytschko *et al*. (2000) and will not be discussed in detail. We rather illustrate the main steps needed in the finite element approximation, i.e., we recast in matrix form the results obtained for the constitutive law in terms of principal stretches. First, we define the coordinate representation of the principal vectors in the two-dimensional setting under consideration as

$$\mathbf{n}_1 = \begin{bmatrix} \cos\alpha \\ \sin\alpha \end{bmatrix}, \qquad \mathbf{n}_2 = \begin{bmatrix} -\sin\alpha \\ \cos\alpha \end{bmatrix}, \tag{33}$$

where the angle $\alpha$ denotes the angle between the first principal direction and axis $x_1$. Using the component form of the (9) the value of $\alpha$ is

$$\alpha = \frac{1}{2}\arctan\left(\frac{2C_{12}}{C_{11}-C_{22}}\right). \tag{34}$$

Next, we choose to order the second Piola-Kirchhoff stress and Green-Lagrange strain tensor components in a vector as $\boldsymbol{S} \rightarrow \mathbf{s}^{\mathrm{T}} = [S_{11}, S_{22}, S_{12}]$, $\boldsymbol{E} \rightarrow \mathbf{e}^{\mathrm{T}} = [E_{11}, E_{22}, 2E_{12}]$, respectively (so that their inner product is preserved). The latter enables to recast the stress spectral decomposition from Eq. (17) as

$$\underbrace{\begin{bmatrix} S_{11} \\ S_{22} \\ S_{12} \end{bmatrix}}_{\mathsf{s}} = \underbrace{\begin{bmatrix} \cos^2\alpha & \sin^2\alpha \\ \sin^2\alpha & \cos^2\alpha \\ \sin\alpha\cos\alpha & -\sin\alpha\cos\alpha \end{bmatrix}}_{\mathsf{T}_{3\times 2}} \underbrace{\begin{bmatrix} s_1 \\ s_2 \end{bmatrix}}_{\mathsf{s}_p}. \tag{35}$$

In the above equation the matrix T is created by ordering the tensor product of eigenvectors (33) in vector notation

$$\mathbf{n}_1 \otimes \mathbf{n}_1 \rightarrow \mathbf{n}_1\mathbf{n}_1^{\mathrm{T}} = \begin{bmatrix} \cos^2\alpha & \cos\alpha\sin\alpha \\ \cos\alpha\sin\alpha & \sin^2\alpha \end{bmatrix} \rightarrow \begin{bmatrix} \cos^2\alpha \\ \sin^2\alpha \\ \cos\alpha\sin\alpha \end{bmatrix}, \tag{36}$$

and putting them as the columns in T (analogously for the $\mathbf{n_2} \otimes \mathbf{n_2}$). Note that the last result for the stress vector(s) can further be directly used for the calculation of the internal force vector of the finite element

$$f_p^{e,int} = \mathbf{e}_i^{\mathrm{T}} \int_{\Omega^e} \mathsf{B}_a^{\mathrm{T}} \mathsf{s}\, \mathrm{d}V, \tag{37}$$

where $a = 1, \ldots, n_{\mathrm{node}}$ denotes the node, $i$ = 1, 2 the degree of freedom ($n_{\mathrm{dof}}$), index $p = n_{\mathrm{dof}}(a - 1) + i$, and matrix B stands for the derivatives of the shape functions.

It is also convenient to write tangent elasticity tensor, given in (19), that connects stress and strain through $\mathbb{C} = \partial \boldsymbol{E}/\partial \boldsymbol{S}$ in a matrix form, using the transformation matrix T from (35), and $D_{\mathrm{ij}}$ from (20)

$$\mathbb{C} \to \mathsf{C}_{(3\times3)} = \mathsf{T} D_{ij} \mathsf{T}^{\mathrm{T}} + \frac{s_1 - s_2}{\lambda_1^2 - \lambda_2^2} \mathsf{g}\mathsf{g}^{\mathrm{T}}. \tag{38}$$

In the above equation auxiliary term $\mathrm{g}^{\mathrm{T}} = [-\sin 2\alpha \quad \sin 2\alpha \quad \cos 2\alpha]$ is used to express the geometric part of the tangent elasticity tensor in more compact form. We note further, that the element tangent stiffness matrix $\boldsymbol{K_e}$ also consists of a material and of a geometric part, and is for the 2D plane elastic membrane finite element given as

$$K_{pq}^{e} = \mathbf{e}_i^{\mathrm{T}} \left[ \int_{\Omega^e} \mathsf{B}_a^{\mathrm{T}} \mathsf{D} \mathsf{B}_b \, \mathrm{d}V + \int_{\Omega^e} \mathsf{G}_{ab} \, \mathrm{d}V \right] \mathbf{e}_j, \tag{39}$$

where $a, b = 1,\ldots, n_{\text{node}}$ denote the node, $i, j = 1, 2$ the degree of freedom, and indexes $p$, and $q$ are $p = n_{\text{dof}}(a - 1) + i$ and $q = n_{\text{dof}}(b - 1) + j$. The geometric part of the tangent stiffness appears only in large displacement problems, and it depends directly on current stress values through

$$\mathsf{G}_{ab} = S_{11} \frac{\partial N_a}{\partial x} \frac{\partial N_b}{\partial x} + S_{22} \frac{\partial N_a}{\partial y} \frac{\partial N_b}{\partial y} + S_{12} \left( \frac{\partial N_a}{\partial x} \frac{\partial N_b}{\partial y} + \frac{\partial N_a}{\partial y} \frac{\partial N_b}{\partial x} \right), \tag{40}$$

where $N_a$ represents element shape function.